Real-structure effects in the dynamical theory of grazing incidence x-ray diffraction

S. A. Stepanov[a] and R. Köhler
MPG-AG "Röntgenbeugung," Hausvogteiplatz 5-7, D-10117 Berlin, Germany

(Received 1 April 1994; accepted for publication 31 August 1994)

A study is presented on the grazing incidence x-ray diffraction in multilayers, with theoretical considerations on the effects of large-scale and small-scale surface and interface roughness and on the effects of interface transition layers. Based on the dynamical theory of grazing incidence x-ray diffraction, the study provides a matrix form of solution for an arbitrary sequence of multilayers. The computations obtained with a developed computer program show the differences that can be observed by the effects of large-scale and small-scale roughness. The effects of small-scale roughness and those of transition layers are similar and thus cannot be separated from each other. But the thickness of surface and interface transition layers or the rms-values of roughness heights are determinable from the shape of diffraction curves by using two different methods. © *1994 American Institute of Physics.*

I. INTRODUCTION

The method of grazing incidence x-ray diffraction (GID) has been effectively applied to studies of semiconductor multilayers.[1–4] However, an interpretation of the measurements was only possible by resorting to the kinematical diffraction theory[5,6] or to relatively crude dynamical diffraction models.[7–9]

Recently a new matrix method has been developed with a view to interpreting GID in arbitrarily layered structures.[10] This method, which is based on the dynamical diffraction approximation provides new possibilities for studying the real-structure effects of GID measurements.

This article is to show how this new approach can be used to explain the effects of large-scale and small-scale surface and interface roughness (Secs. III and IV) as well as those of the transition layers at multilayer interfaces (Sec. V). The short outline on the theory[10] given in Sec. II is intended for initiating the discussion.

II. OVERVIEW OF MATRIX METHOD

Consider GID in a multilayered structure composed of N arbitrary amorphous and matched crystalline layers arranged on a thick substrate (Fig. 1). The dynamical diffraction equations for GID in this structure can be reduced to the following matrix form (for any polarization of the incident wave):

$$
\begin{aligned}
S^v F^{v(L)} E^v &= S^1 F^{1(U)} D^1 \\
S^1 F^{1(L)} D^1 &= S^2 F^{2(U)} D^2 \\
\cdots &= \cdots \\
S^k F^{k(L)} D^k &= S^{k+1} F^{k+1(U)} D^{k+1} \\
\cdots &= \cdots \\
S^N F^{N(L)} D^N &= S^s F^{S(U)} D^s \,.
\end{aligned}
\qquad (1)
$$

Here S and F are (4×4) matrices representing layer characteristics; E and D are four-component vectors composed of x-ray wave amplitudes that have to be determined: $E^v=(1,0,E_s,E_h)$, where E_s and E_h are the amplitudes of reflected and diffracted x-ray waves in vacuum, and $D^k=(D_1^k,D_2^k,D_3^k,D_4^k)$, where D_j^k are x-ray wavefield amplitudes in the kth layer. Matrices $F^{k(L,U)}$ are diagonal and contain x-ray phase exponentials calculated at layer boundaries: $F_{ij}^{k(L,U)}=F_i^{k(L,U)}\delta_{ij}$, where we denoted $F_i^{k(L,U)} \equiv \exp(iu_i^k k_0 z^{(L,U)})$; k_0 is the module of the x-ray wave vector in vacuum and z is the coordinate along the internal surface normal. Indices $z^{(L)}$ and $z^{(U)}$ indicate that the coordinate is taken from the lower or upper boundary of the layer.

The parameters u_j^k are the roots of the fourth-order dispersion equation of dynamical diffraction in the kth layer: $(u_j^{k2}-\Phi_0^2-\chi_0^k)((u_j^k+\psi)^2-\Phi_h^2-\chi_0^k)=\chi_h^k\chi_{\bar{h}}^k$. These roots are assumed to be sorted in decreasing order of Im u_j. The parameter $\psi=2\varphi\sin\theta_B$ is the effective misorientation angle; Φ_0, Φ_h, and φ are the grazing angles of incident wave, diffracted wave, or Bragg reciprocal lattice vector in relation to the surface respectively. Parameters χ_0^k, χ_h^k, $\chi_{\bar{h}}^k$

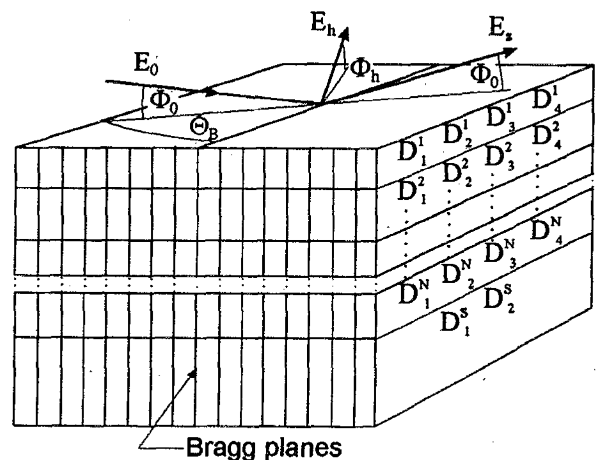

FIG. 1. Schematic view of x-ray grazing-incidence diffraction in multilayers. E_0, E_h, and E_s are the amplitudes of the incident, Bragg diffracted, and specularly reflected waves. D_1^N–D_4^N are the wavefield amplitudes in an arbitrary Nth layer. D_1^s and D_2^s are the wavefield amplitudes in the substrate. Φ_0 and Φ_h are the angles of incidence and exit; θ_B is the Bragg angle.

[a]Permanent address: Institute for Nuclear Problems, Minsk SU-220050, Republic of Belarus.

are Fourier components of the x-ray dielectric susceptibility of the kth layer.

Finally, matrices S^k have the following form:

$$S_{ij}^k = \begin{pmatrix} Y_1^k & Y_2^k & Y_3^k & Y_4^k \\ V_1^k & V_2^k & V_3^k & V_4^k \\ Y_1^k u_1^k & Y_2^k u_2^k & Y_3^k u_3^k & Y_4^k u_4^k \\ V_1^k(u_1^k+\psi) & V_2(u_2^k+\psi) & V_3^k(u_3^k+\psi) & V_4^k(u_4^k+\psi) \end{pmatrix}, \quad (2)$$

where $Y_j=1$, $V_j=(u_j^2-\Phi_0^2-\chi_0)/\chi_h$ for crystalline layers and $Y_1=Y_3=V_2=V_4=1$, $Y_2=Y_4=V_1=V_3=0$ for amorphous layers and vacuum.

For the substrate layer the roots with Im $u_j<0$ are discarded and therefore only the first 2 components of vector D and the first 2 rows of matrix S remain and the size of F^s is (2×2).

The solution of Eq. (1) for perfect multilayer structure is straightforward. At first, these equations are transformed to the form:

$$\begin{aligned} E^v &= (F^{v(L)})^{-1}(S^v)^{-1}S^1F^{1(U)}D^1 \\ D^1 &= (F^{1(L)})^{-1}(S^1)^{-1}S^2F^{2(U)}D^2 \\ \cdots &= \cdots \\ D^k &= (F^{k(L)})^{-1}(S^k)^{-1}S^{k+1}F^{k+1(U)}D^{k+1} \\ \cdots &= \cdots \\ D^N &= (F^{N(L)})^{-1}(S^N)^{-1}S^sF^{S(U)}D^s. \end{aligned} \quad (3)$$

Thus we obtain:

$$E^v = \underbrace{(F^{v(L)})^{-1}(S^v)^{-1}S^1F^{1(U)}(F^{1(L)})^{-1}(S^1)^{-1}\cdots S^NF^{N(U)}(F^{N(L)})^{-1}(S^N)^{-1}S^sF^{s(U)}}_{\tilde{S}}D^s, \quad (4)$$

where $\tilde{S}$ is a (2×4) matrix and Eq. (4) is a set of 4 linear algebraic equations with respect to 4 unknown variables: E_s, E_h, D_1^s, and D_2^s. The solution for E_h is:

$$E_h=\frac{\tilde{S}_{41}\tilde{S}_{22}-\tilde{S}_{42}\tilde{S}_{21}}{\tilde{S}_{11}\tilde{S}_{22}-\tilde{S}_{12}\tilde{S}_{21}}, \quad (5)$$

and the reflection coefficient for the diffracted wave is calculated according to the formula:

$$P_h=(\Phi_h/\Phi_0)|E_h|^2. \quad (6)$$

Figure 2 presents the application of above algorithm to the computation of a GID curve for an AlAs/GaAs superlattice (SL) consisting of 20 periods of 150 Å GaAs and 100 Å AlAs matched layers arranged on a crystalline GaAs substrate. The parameters of computation are: x-ray wavelength $\lambda=2\pi/k_0=1.5$ Å, (220) diffraction planes, $\varphi=0$, $\Phi_0=30'$, π-polarization. The curve plotted in dependence of Φ_h shows sharp oscillations due to SL resonances. In the following we demonstrate how various imperfections in SL structure affect this example.

III. EFFECT OF LARGE-SCALE ROUGHNESS

The effect of large-scale surface roughness on x-ray specular reflection curves was studied in many papers (see, for example, recent reports[11,12]). This effect is usually considered by averaging x-ray intensities over surface misorientations with a Gaussian weight function. This procedure will be valid if the surfaces are locally flat on a length scale $\leqslant 1/\Delta k_0 \simeq 1/(2k_0\sqrt{|\chi_0|})$, where Δk_0 is the change in x-ray wave vector under specular reflection (see, e.g., Ref. 4). It has been shown that the same approach is applicable to GID intensities.[13] Though the formulas for averaging are provided in Ref. 13, the computations were not carried out and here for the first time we present the dynamical diffraction calculations. Recently, the effect of large-scale surface roughness on GID has been computed in the kinematical diffraction approximation.[14]

Assuming that a surface domain is misoriented with respect to the mean surface position by angles θ_1 and θ_2, where θ_1 is measured in the incidence direction and θ_2 in that perpendicular to θ_1, then diffraction angles at this domain are modified as follows:

$$\Phi_0=\tilde{\Phi}_0+\theta_1,$$

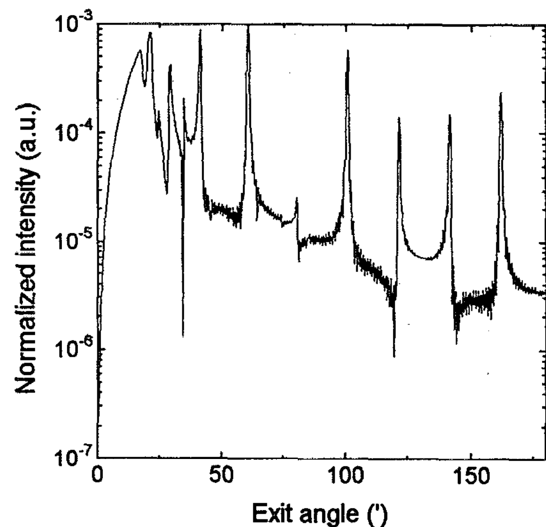

FIG. 2. GID curve for a perfect SL computed with the matrix method depending on the exit angle of diffracted waves.

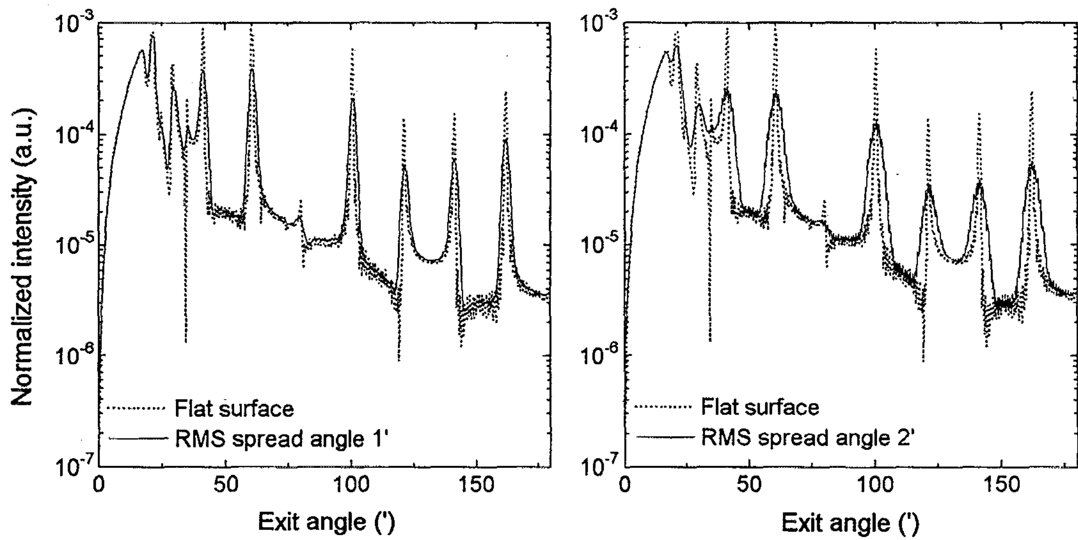

FIG. 3. The effect of large-scale roughness on GID curves for angular spreads of 1′ and 2′ rms.

$$\Phi_h=\tilde{\Phi}_h+\theta_1 \cos 2\theta_B+\theta_2 \sin 2\theta_B,$$
$$\varphi=\tilde{\varphi}-\theta_1 \sin \theta_B+\theta_2 \cos \theta_B, \tag{7}$$

where $\tilde{\Phi}_0$, $\tilde{\Phi}_h$, $\tilde{\varphi}$ are the mean values and θ_B is the Bragg angle.

The averaged intensity is calculated as:

$$\langle P_h(\tilde{\Phi}_0,\tilde{\Phi}_h)\rangle \sim \int\int d\theta_1 d\theta_2 P_h(\Phi_0,\Phi_h,\varphi) \times \exp(-(\theta_1^2+\theta_2^2)/2\theta_{\rm lr}^2), \tag{8}$$

where $\theta_{\rm lr}$ is the rms angle of surface misorientations.

If $\theta_{\rm lr}$ is small (usually less than 1′), the change of φ in Eq. (7) can be neglected[14] and integration is reduced to averaging over Φ_0 and Φ_h in Eq. (8).

Results of computations are presented in Fig. 3. The distinct broadening of SL peaks at $\theta_{\rm lr}=1'$ and $\theta_{\rm lr}=2'$ is well seen. Thus, in the case of SL the large-scale roughness can be simply estimated from SL peak halfwidths and taken into account in theoretical simulations.

IV. EFFECT OF SMALL-SCALE ROUGHNESS

The small-scale roughness effect on GID was considered only within kinematical diffraction theory.[5,14] However, the methods of accounting for roughness developed in x-ray specular reflection studies (see, e.g. Refs. 11, 12, 15, and 16) can be applied to the dynamical diffraction model described in Sec. II. In contrast to the averaging procedure for the large-scale roughness x-ray wave amplitudes are averaged here instead of x-ray intensities due to the assumption that the lateral roughness scale is much less than $1/\Delta k_0$.

Supposing that the coordinates $z_{k+1}^{(U)}\equiv z_k^{(L)}$ of interfaces in Eq. (4) are random functions of lateral coordinates (x,y) we get:

$$z_k(x,y)=\langle z_k\rangle+\Delta z_k(x,y), \tag{9}$$

where Δz_k are small values.

The present work is confined only to the study of the roughness effect on coherent scattering. No diffuse scattering due to roughness (i.e., x-ray intensities in incoherent scattering directions) is considered. This is reasonable because GID intensities are usually measured not far from the Bragg maximum rather than at large Φ_0 and Φ_h values where the diffusely scattered intensities are likely to become comparable with the coherent intensities.

As shown in Ref. 12, the averaging over (x,y) for coherent scattering directions yields always Gaussian averages over Δz, irrespective of the form of the lateral roughness correlation function $\langle[\Delta z(x',y')-\Delta z(x,y)]^2\rangle$:

$$\langle E^v\rangle=\frac{1}{\sqrt{2\pi}\sigma}\int_{-\infty}^{\infty} dz E^v(z)\exp(-z^2/2\sigma^2), \tag{10}$$

where σ is the rms roughness height.

A. Effect of surface roughness

Let us consider at first a perfect crystal with a rough surface. The matrix $\tilde{S}$ for this case can be written in the form:

$$\tilde{S}_{ij}=(F_i^{v(L)})^{-1}X_{ij}F_j^{1(U)}=\exp[i(u_j^1-u_i^v)k_0z]X_{ij}, \tag{11}$$

where $X_{ij}\equiv\{(S^v)^{-1}S^s\}_{ij}$.

Using Eqs. (11) in (5) we obtain:

$$E_h=\frac{X_{41}X_{22}-X_{42}X_{21}}{X_{11}X_{22}-X_{12}X_{21}} \exp[i(u_1^v-u_4^v)k_0z]. \tag{12}$$

Then, substituting Eq. (12) in the average integral (10) and taking into account that $u_1^v=\Phi_0$ and $u_4^v=-\Phi_h-\psi$ we obtain:

$$\langle E_h\rangle=E_h^{\rm Perf}\exp[-k_0^2\sigma^2(\Phi_0+\Phi_h+\psi)^2/2]. \tag{13}$$

In the same way:

$$\langle E_s\rangle=E_s^{\rm Perf}\exp[-k_0^2\sigma^2(2\Phi_0)^2/2]. \tag{14}$$

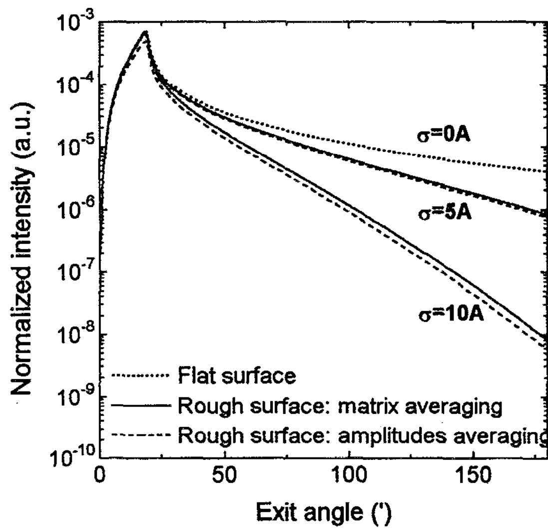

FIG. 4. The effect of small-scale surface roughness on GID curves taken from a substrate at rms heights 5 Å and 10 Å. Two different approaches give very similar results.

Equation (14) shows that the roughness effect on the specularly reflected beam in GID coincides with that on the usual x-ray specular reflection without any Bragg diffraction (compare, e.g., this equation with the corresponding formulas in Refs. 12, 11, and 17).

Equation (13) shows that roughness effect on the diffracted beam depends on both angles Φ_0 and Φ_h. Besides, at first sight it may seem strange that the roughness effect in Eq. (13) depends on ψ. However, one should remember the relation: $\Phi_h^2=(\Phi_0\pm\psi)^2-\alpha$, where α is the deviation from the Bragg condition. Due to this relation the term in the exponent may be written in the form: $\Phi_0+\Phi_h+\psi=\Phi_h\mp\Phi_h^{\mathrm{Br}}$, where Φ_h^{Br} is the value of Φ_h at $\alpha=0$. Obviously, at the transition from GID to ordinary Bragg-case diffraction ($\psi<0$, $|\psi|\gg\sqrt{|x_0|}$) the parameter Φ_h^{Br} becomes negative and we arrive at the well-known result that the roughness effect is only essential for the tails of the Bragg curve.[18,19]

Thus, we realize that the effect of small-scale surface roughness on GID curves is analogous to that on x-ray specular reflection curves. The surface roughness is displayed on GID curves as a Debye–Waller factor that attenuates the intensity at large values of Φ_0 and Φ_h. Figure 4 shows the calculations for $\sigma=0$ (dotted line), $\sigma=5$ Å and $\sigma=10$ Å (dashed lines). It is obvious that σ can be easily determined from the overall damping rate of the curves.

However, as shown in Ref. 12, roughness is duly considered in the above procedure by using the Born approximation. The application of the distorted-wave Born approximation (DWBA), which is more consistent at grazing angles, yields slightly different results near the critical angle of x-ray specular reflection $\Phi_c=\sqrt{|x_0|}$ which is much better in line with experimental data.[12,15]

In Refs. 11 and 17 where the equations for x-ray specular reflection from layered media were presented in a matrix form similar to Eq. (4), it has been shown that the use of DWBA is equivalent to averaging individual coefficients in the matrix $\tilde{S}$. Physically, this means that "the coherency of the x-ray field at the rough interface is lost: the incoming and the reflected amplitudes each suffer a phase randomization, independent of one another."[16]

Now, we try to extend the latter procedure to GID. Carrying out averaging in Eq. (11) we obtain:

$$\langle\tilde{S}_{ij}\rangle=\tilde{S}_{ij}^{\mathrm{Perf}}\exp[-k_0^2\sigma^2(u_j^1-u_i^v)^2/2]. \tag{15}$$

Thus, in the latter case every element in matrix $\tilde{S}$ is multiplied by the Debye–Waller factor that contains the difference between wave propagation parameters in both media. Therefore, the roughness effect will be decreased if this difference is decreased. This is a physically consistent result, whereas that provided by Eqs. (13) and (14) is not.

The respective calculations are presented in Fig. 4 (solid lines) for $\sigma=5$ Å and $\sigma=10$ Å. It is well seen that both roughness averaging algorithms provide very similar results at large Φ_h. At $\Phi_h<\Phi_c$ the former one shows a roughness effect (see the dashed lines) whereas the latter one does not. Principally, the experiment should decide which model is appropriate. However, from our experience we should expect that the latter one would fit better. Therefore, in the following we shall deal with the latter model.

B. Effect of interface roughness

Now we consider multilayers where all interfaces are rough with rms roughness heights σ_k ($k=1,\ldots,N$). In the general case the averaging of matrix $\tilde{S}$ should account for the correlations between roughnesses at different interfaces, while the averaging integral could be represented as a sum of terms containing different interface-to-interface correlation functions.

Here we analyze the particular case of roughness without correlation between different interfaces. Then averaging can be performed separately at every interface because the exponents at the other interfaces can be moved outside of the integration sign. Therefore, integration can be directly implemented in Eq. (3).

We denote $(S^k)^{-1}S^{k+1}\equiv X^{k,k+1}$. Then, any equation from Eq. (3) can be written:

$$D^k=(F^{k(L)})^{-1}X^{k,k+1}F^{k+1(U)}D^{k+1}. \tag{16a}$$

A more detailed form of this equation is ($z_{k+1}^{(U)}=z_k^{(L)}\equiv z$):

$$D_i^k=\mathrm{e}^{-iu_i^k k_0 z}\delta_{ij}X_{jm}^{k,k+1}\mathrm{e}^{iu_m^{k+1}k_0 z}\delta_{mn}D_n^{k+1}$$
$$=X_{ij}^{k,k+1}\mathrm{e}^{i(u_j^{k+1}-u_i^k)k_0 z}D_j^{k+1}, \tag{16b}$$

where the summation over all repeated indices is assumed.

Averaging over $\Delta z(x,y)$ both sides of Eq. (16b) and assuming Gaussian roughness spread we obtain:

$$\langle D_i^k\rangle=\langle X_{ij}^{k,k+1}\rangle\mathrm{e}^{i(u_j^{k+1}-u_i^k)k_0}D_j^{k+1}, \tag{17}$$

where

$$\langle X_{ij}^{k,k+1}\rangle=X_{ij}^{k,k+1}\exp[-k_0^2\sigma_k^2(u_j^{k+1}-u_i^k)^2/2]. \tag{18}$$

It follows from Eq. (18) that in case of interface roughness every element of the matrix product $(S^k)^{-1}S^{k+1}$ is multiplied by the respective Debye–Waller attenuating factor.

In order to explain the physics of this attenuation, we now suppose that x-ray scattering in layers A and B does not differ very much, i.e., the roots u_j^k and u_j^{k+1} are close to each other. Then the matrices S^k and S^{k+1} are also close to each other and the matrix $X^{k,k+1} \equiv (S^k)^{-1}S^{k+1}$ is close to a unit matrix (the diagonal elements are close to one and the modules of all nondiagonal elements are much less than one). In this case the Debye–Waller exponents containing $(u_j^{k+1}-u_i^k)^2$ suppress only nondiagonal elements of $X^{k,k+1}$, whereas the diagonal elements remain unchanged. As a result, $X^{k,k+1}$ moves closer to the diagonal unit matrix and the interface effect is shadowed. Particularly, in case of SL, the amplitudes of SL peaks on GID curves are decreased.

The small-scale roughness effect on GID curves in case of a SL is shown in Figs. 5–6. There is a general difference between the effects of surface and interface roughness. The surface roughness basically gains the attenuation of overall GID intensity at large angles. This is obviously the same effect as on the curves taken from a rough substrate (compare with Fig. 4). In contrast to that the interface roughness does not change the overall intensity drop with increasing angle, but reduces the peak intensity of high-order SL peaks.

As is well seen in the figures, the effect of surface roughness is stronger than that of interface roughness. Particularly, the increase in SL peak intensities is noticeable due to surface roughness. The comparatively strong effect of surface roughness is not surprising because the same effect has been reported for x-ray specular reflection curves of SLs.[17] The physical explanation may be that the difference in χ_0 between vacuum and SL is much larger than that between the pair of layers of SL. Therefore, the surface interface plays the dominant role. If this interface is smoothed, the role of the SL interfaces will be effectively increased together with the height of SL peaks that are increased as well.

V. EFFECT OF TRANSITION LAYERS

The smooth transitions between layers in multilayer structure may be formed, e.g., due to interdiffusion. On the other hand, many studies of effect of small-scale surface roughness on x-ray specular reflection curves have reported that small-scale roughness could be described as a transition layer[11,12,16,17] and, consequently, the effects of surface roughness and transition layers are indistinguishable. Therefore, the general question is whether or not these two types of distortion can be separated by GID.

The effect of transition layers is directly included in the model described in Sec. II. To account for this effect we can follow the approach proposed by Underwood and Barbee[20] for x-ray specular reflection from multilayers. Let χ_0^A and χ_h^A be the x-ray susceptibilities of layer A and χ_0^B and χ_h^B that of layer B. In Ref. 20 it was suggested that the transition layer should be represented as a sequence of N^{Tran} thin sublayers with constant susceptibilities $\chi_0^{\mathrm{Tran}(i)}$ and $\chi_h^{\mathrm{Tran}(i)}$ within every layer:

$$\chi_{0,h}^{\mathrm{Tran}(i)} = \chi_{0,h}^A f_i + \chi_{0,h}^B (1-f_i), \qquad (19)$$

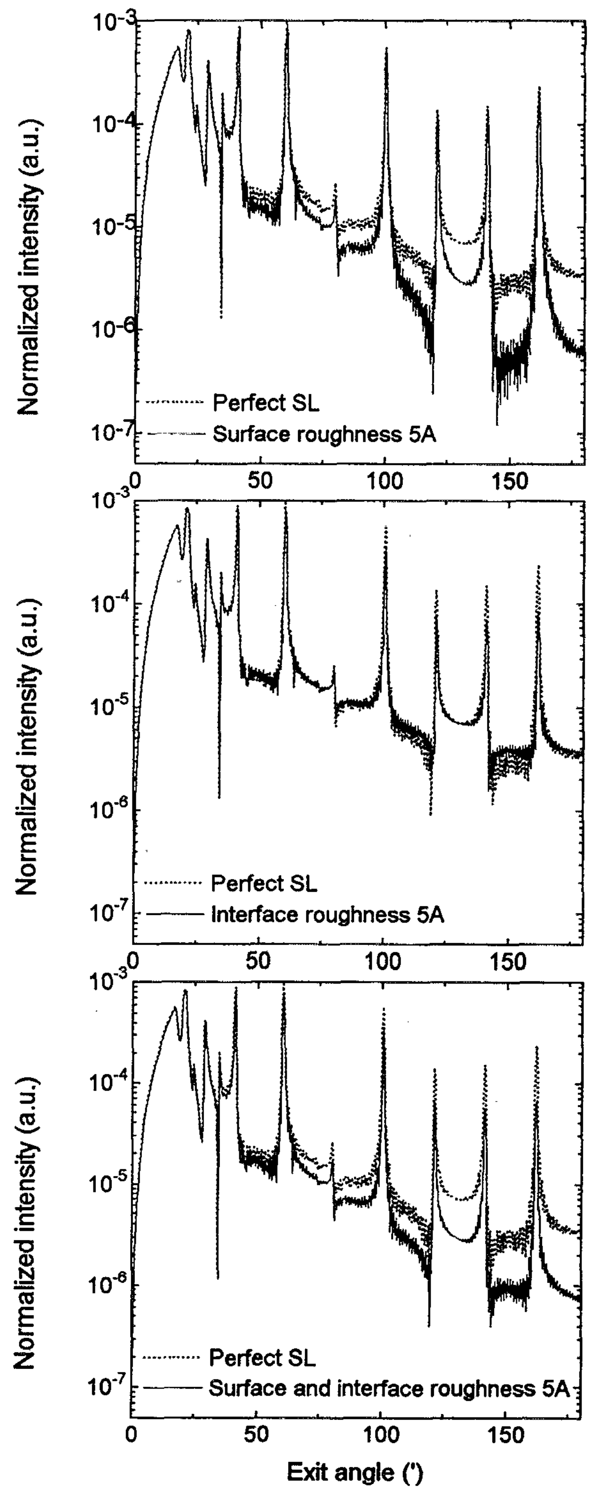

FIG. 5. The effect of 5 Å small-scale roughness on GID curves of a SL at different combinations of surface and interface roughness.

where f_i are the transition coefficients varying from 0 to 1 on the transition interval $2t_{1/2}^{\mathrm{Tran}}$. For cosinelike transition these coefficients can be expressed:

$$f_i = \{1+\cos(\pi\Delta z_i/2t_{1/2}^{\mathrm{Tran}})\}/2 = \cos^2(\pi\Delta z_i/4t_{1/2}^{\mathrm{Tran}}).$$

The parameter Δz_i is the sublayer coordinate varying from zero to $2t_{1/2}^{\mathrm{Tran}}$.

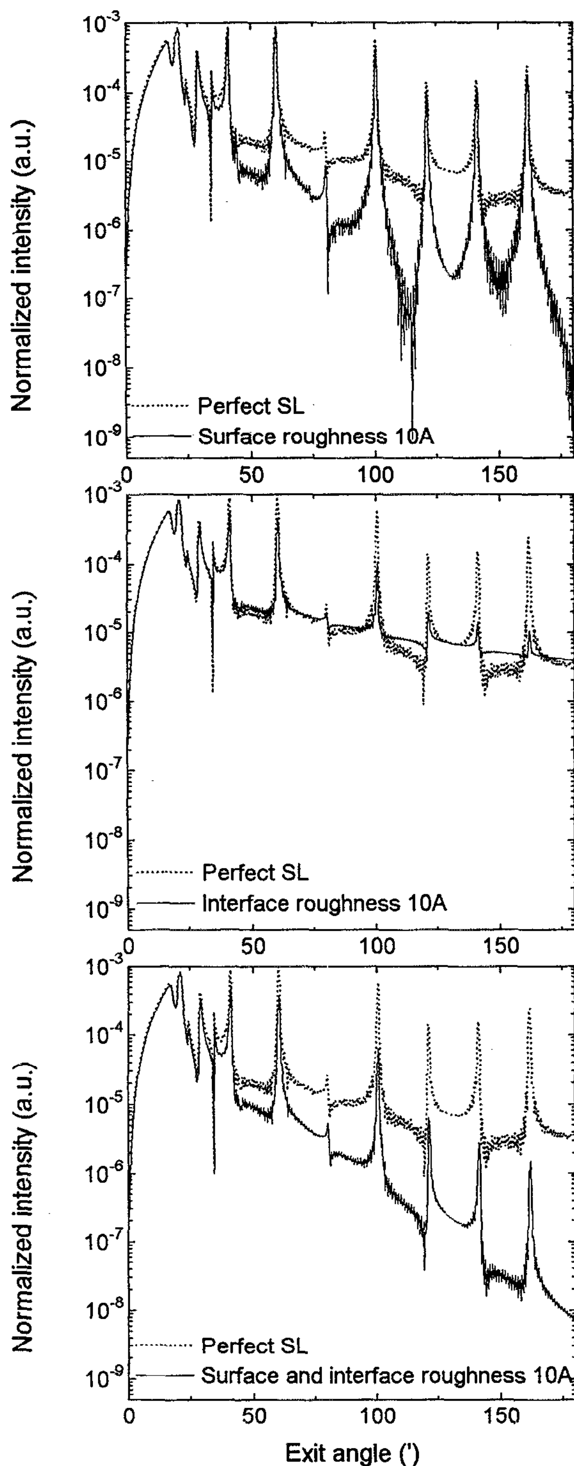

FIG. 6. As Fig. 5, but for 10 Å small-scale roughness.

First of all, the roughness and transition layer effects on substrate measurements are compared in Fig. 7. At $t_{1/2}^{\mathrm{Tran}}=2\sigma$ both effects virtually coincide and therefore they cannot be distinguished.

On the other hand, the curve with $t_{1/2}^{\mathrm{Tran}}=20$ Å shows a drop at $\Phi_h \sim \lambda/2t_{1/2}^{\mathrm{Tran}}$, whereas the respective curve with $\sigma=10$ Å does not show it. Apparently, the model used in Sec.

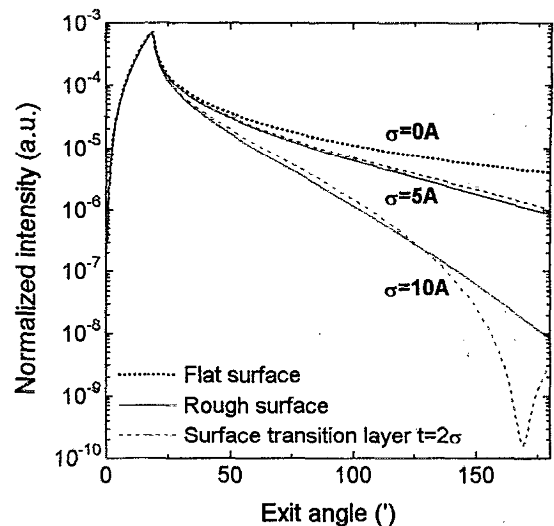

FIG. 7. Comparison of small-scale surface roughness and transition layer effects on GID curves computed for a substrate.

IV is not applicable because it is based on the assumption of a small exponent: $k_0\sigma\Phi \ll \pi$.

The same perfect coincidence of small-scale roughness and transition layers effects at $t_{1/2}^{\mathrm{Tran}}=2\sigma$ is maintained except for large $k_0\sigma\Phi$ in case of SL.

Thus, the effects of small-scale roughness and transition layers cannot be distinguished with GID measurements. Therefore, both methods developed in Secs. IV and V can be successfully applied to the description of these effects. For small $t_{1/2}^{\mathrm{Tran}}$ or σ the roughness approach is preferable because it is much faster. Conversely, for large $t_{1/2}^{\mathrm{Tran}}$ or σ the transition layer approach is more reliable because it corresponds to the dynamical diffraction approximation.

As is well known, the difference between the roughness and smooth transition layers can be detected with diffuse scattering measurements.[12] However, at present we do not see any advantage of diffuse scattering measurements in GID experiments. Therefore, it is much simpler to carry out these measurements in usual X-ray specular reflection experiments far from GID conditions. The information obtained will complement the GID measurements.

VI. CONCLUSIONS

Effects of surface and interface roughness and transition layers on GID curves taken from multilayers have been studied. Large-scale roughness causes the broadening of curves and can be easily determined especially for SL measurements. Small-scale roughness and the interface transition layers result in the same variations of GID curves and cannot be separated from each other. However, the parameters of surface and interface smoothing (either the transition layer thickness or the roughness height) can be determined from the shape of GID curves by two independent methods which provide an increased reliability of measurements.

[1] A. L. Golovin, R. M. Imamov, and O. G. Melikyan, J. Appl. Cryst. **22**, 406 (1989).
[2] O. G. Melikyan, R. M. Imamov, and D. V. Novikov, Fiz. Tverdogo Tela (USSR) **4**, 1572 (1992).
[3] H. Rhan, U. Pietsch, S. Rugel, H. Metzger, and J. Peisl, J. Appl. Phys. **74**, 146 (1993).
[4] U. Pietsch, H. Metzger, S. Rugel, B. Jenichen, and I. K. Robinson, J. Appl. Phys. **74**, 2381 (1993).
[5] T. Baumbach, V. Holy, U. Pietsch, and M. Gailhanou, International Conference X-ray and Neutron Surface Scattering Collect. Abstract, Dubna, 1993 (unpublished).
[6] O. G. Melikyan, Kristallografiya **36**, 549 (1991).
[7] P. A. Aleksandrov, A. M. Afanas'ev, M. K. Melkonyan, and S. A. Stepanov, Phys. Status Solidi A **81**, 47 (1984).
[8] P. A. Aleksandrov, A. M. Afanas'ev, A. L. Golovin, R. M. Imamov, D. V. Novikov, and S. A. Stepanov, J. Appl. Cryst. **18**, 27 (1985).
[9] P. A. Aleksandrov, A. M. Afanas'ev, and S. A. Stepanov, Phys. Chem. Mech. Surf. **3**, 2222 (1985).
[10] S. A. Stepanov, Kristallografiya **39**, 221 (1994).
[11] E. E. Fullerton, J. K. Schuller, H. Vanderstraeten, and Y. Bruynseraede, Phys. Rev. B **45**, 9292 (1992).
[12] S. K. Sinha, E. B. Sirota, S. Garoff, and H. B. Stanley, Phys. Rev. B **38**, 2297 (1988).
[13] R. M. Imamov, E. A. Kondrashkina, D. V. Novikov, and S. A. Stepanov, Kristallografiya **32**, 852 (1987).
[14] G. Wallner, C. Landesberger, H. Metzger, J. Peisl, and S. Rugel, Phys. Status. Solidi A **135**, 73 (1993).
[15] L. Nevot and P. Croce, Rev. Phys. Appl. **15**, 761 (1980).
[16] F. Stanglmeier, B. Lengeler, W. Weber, H. Göbel, and M. Schuster, Acta Cryst. A **48**, 626 (1992).
[17] Z. H. Ming, A. Krol, Y. L. Soo, Y. H. Kao, J. S. Park, and K. L. Wang, Phys. Rev. B **47**, 16373 (1993).
[18] P. A. Aleksandrov, A. M. Afanas'ev, and M. K. Melkonyan, Kristallografiya **26**, 1275 (1981).
[19] A. M. Afanas'ev, P. A. Aleksandrov, R. M. Imamov, A. A. Lomov, and A. A. Zavyalova, Acta Cryst. A **40**, 352 (1984).
[20] J. H. Underwood and T. W. Barbee, Appl. Opt. **20**, 3027 (1981).